Received: 30 April 2019 | Revised: 6 November 2019 | Accepted: 15 November 2019 | Published on: 23 December 2019

DOI: 10.1002/met.1864

RESEARCH ARTICLE

Meteorological Applications RMetS

Improving the weighted mean temperature model: A case study using nine year (2007–2015) radiosonde and COSMIC data in Hong Kong

Pengfei Xia[1,2] | **Shirong Ye**[1] | **Biyan Chen**[3] | **Dezhong Chen**[1,2] | **Keke Xu**[4]

[1]GNSS Research Centre, Wuhan University, Wuhan, China

[2]School of Geodesy and Geomatics, Key Laboratory of Geospace Environment and Geodesy, Ministry of Education, Wuhan University, Wuhan, China

[3]School of Geosciences and Info-Physics, Central South University, Changsha, China

[4]School of Surveying and Land Information Engineering, Henan Polytechnic University, Jiaozuo, China

Correspondence
Pengfei Xia and Shirong Ye, GNSS Research Center, Wuhan University, No.129 Luoyu Road, Hongshan, Wuhan, Hubei, China.
Email: pfxia130@whu.edu.cn (P. X.) and srye@whu.edu.cn (S. Y.)

Funding information
China Postdoctoral Science Foundation, Grant/Award Number: 2019M652706; Henan Science and Technology Public Relations, Grant/Award Number: 172102310178; National Natural Science Foundation of China, Grant/Award Number: 41904025; 41974031; 41905027; the Fundamental Research Funds for the Central Universities, Grant/Award Number: 2042019kf0032

Abstract

The important role of a humidity conversion factor in mapping the zenith wet delay (ZWD) onto precipitable water vapour (PWV) makes it a vital parameter in Global Navigation Satellite System (GNSS) meteorology. The accuracy of the humidity conversion factor depends mainly on the quality of the atmospheric weighted mean temperature (T_m) calculation. Several effective models have been developed to calculate T_m with parameters such as the station's location, date of measurement and surface temperature. However, the drawbacks of these models, including low accuracy in some areas and complex model functions, cannot be ignored because they prevent further application in atmosphere analysis. Therefore, a new discrete integral formula for highly accurate calculation of T_m is proposed. Moreover, the linear relationships between time, surface temperature (T_s), height (H) and T_m are well studied based on radiosonde and Constellation Observation System for Meteorology Ionosphere and Climate (COSMIC) historical data (2007–2015). A new regional T_m model was investigated on the basis of parameters time, T_s and H in Hong Kong, China. The evaluation results indicate that the improvement of T_m derived from the new integral is > 4.6 K based on radiosonde data. In addition, the statistical results of T_m with different sampling based on radiosonde data and a COSMIC "wetPrf" profile show that the improvement of T_m derived from the new integral are > 2.10 and 2.75 K, respectively. Finally, wetPrf profiles collocated with Hong Kong and the 45,004 radiosonde station collected from January 1 to October 31, 2016, are used to evaluate the accuracy of the new T_m model. Compared with the Bevis model, the statistical results indicate that the T_m accuracy is improved by 34.75%. Therefore, the model for T_s and time is suggested to estimate the T_m in Hong Kong.

KEYWORDS

atmospheric weighted mean temperature, COSMIC, GNSS, meteorology, humidity conversion factor, radiosonde

1 | INTRODUCTION

Water vapour, an important element of the Earth's atmosphere concentrated mainly at the base of the Troposphere, is vital for weather forecasting (Hamill and Church, 2000). Traditionally, balloon-based radiosonde soundings, microwave radiometers and radio occultation (RO) products are used to study the temporal and spatial variation of atmospheric water vapour (Askne and Nordius, 1987; Brettle and Galvin, 2003). However, due to their high costs, low spatial and temporal resolution, and heavy workload, these approaches cannot meet the increasing requirements of meteorological development (Brettle and Galvin, 2003). Global Navigation Satellite System (GNSS) meteorology can effectively compensate for the shortcomings of these traditional methods (Yao et al., 2013, 2014).

Tropospheric delay is one of the most important sources of error and bias in the GNSS signal propagation (Kouba and Héroux, 2001). The delay contains two parts: hydrostatic and wet (Davis et al., 1985). The latter usually is used in the GNSS meteorology (Bevis et al., 1992). The tropospheric zenith delay (ZTD) can usually be estimated using a GNSS double-difference, single-difference or undifferenced processing strategy (Zumberge et al., 1997; Kouba and Héroux, 2001; Alber et al., 2000; Braun et al., 2001); hydrostatic zenith delay (ZHD) can be precisely obtained based on empirical models such as the Saastamoinen model (Saastamoinen, 1972), the Black model (Black, 1978), and the Hopfield model (Hopfield, 1971). Zenith wet delay (ZWD) can be derived by subtracting the ZHD from the ZTD. Finally, the precipitable water vapour (PWV) can be computed from the ZWD using the humidity conversion factor (Bevis et al., 1992). The relationship between the ZWD and the PWV is expressed as (Bevis et al., 1992):

$$\mathrm{PWV} = \Pi \cdot \mathrm{ZWD} \tag{1}$$

where Π refers to the humidity conversion factor, which can be expressed as a function of the atmospheric weighted mean temperature (T_m) (Bevis et al., 1992):

$$\Pi = \frac{10^6}{\rho_w \cdot \frac{R}{m_w} \cdot \left[\frac{k_3}{T_m} + k_2 - \frac{m_w}{m_d} \cdot k_1\right]} \tag{2}$$

where ρ_w denotes the density of liquid water; k_1, k_2 and k_3 are constants: k_1 = 77.6 K·hPa^{-1}, k_2 = 70.4 K·hPa^{-1} and $k_3 = 3.739*10^5$ K·hPa^{-1} (Davis et al. 1985; Bevis et al. 1994); m_d and m_w are the molar masses of dry atmosphere and vapour, respectively; R is the universal gas constant; and T_m is the atmospheric weighted mean temperature.

Equations (1) and (2) show that when the solution of the ZWD is confirmed, the accuracy of the PWV depends mainly on the humidity conversion factor, which is used for mapping the ZWD to the PWV. The accuracy of the humidity conversion factor depends mainly on the quality of the atmospheric weighted mean temperature (T_m); therefore, the T_m is a vital parameter in the ground-based GNSS atmospheric research. Bevis et al. (1992) first established the one-dimensional linear relationship between the T_m and surface temperature (T_s) based on historical radiosonde products, and this model was suitable for use in mid-latitude areas. Ross and Rosenfeld (1997) verified that the relationship between the T_m and T_s would change in different areas and seasons. Gu et al. (2005) studied the regional variations of the T_m. Moreover, a regional linear model was constructed between the T_m and T_s (Li et al., 1999; Liu et al., 2000; Wang et al., 2007; Lv et al., 2008). Yao et al. (2012, 2013) established the global T_m model with ground-based radiosonde data, which requires only the date as an input. However, these traditional models are one-dimensional linear models that can only consider either the surface temperature or the time variable, such as cosine function models that only consider time.

In the present study, the aim is to establish a high-precision regional T_m model based on radiosonde and Constellation Observation System for Meteorology Ionosphere and Climate (COSMIC) historical data for Hong Kong, China. In the proposed model, the mathematical function used to derive the T_m was optimized with radiosonde and COSMIC data. The T_s, height and time parameters were considered in the new T_m model, and a quadratic function was used to estimate the relationship between the new model and the T_s as well as the relationship between the new model and height. Moreover, the trigonometric function relation was applied to elucidate the relationship between the new model and the time variable. Finally, the radiosonde- and COSMIC-derived T_m were used as references to evaluate the optimized model, and the results were compared and discussed.

The paper is organized as follows. Section 2 introduces the improved method to obtain the T_m from the radiosonde and COSMIC data. Section 3 describes the process of estimating the new T_m model. Section 4 presents the validation of the new model. The conclusions are presented in Section 5.

2 | METHODS

The weighted mean temperature of the atmosphere varies significantly with time and area, and the global T_m models are not accurate enough in some areas. To solve

the weakness of the traditional T_m calculation, a new method to model the regional T_m is proposed with the use of radiosonde and RO data. Davis et al. (1985) proposed a T_m calculation model that integrates temperature and water vapour pressure with the respective height. The atmospheric products derived from radiosonde and RO provide high vertical resolution of the temperature and water vapour profiles and allow the estimation of the T_m by traditional means. However, the traditional linear discrete methods would cause some errors in the T_m estimation, because water vapour pressure usually follows an exponential distribution in the vertical direction. Thus, a new method to discretize the integral for the T_m calculation is proposed.

When the GNSS radio signals travel through the atmosphere, they are delayed by the Troposphere. This tropospheric delay can usually be divided into two parts: a hydrostatic component and a wet component. After subtracting the ZHD from the ZTD, the obtained ZWD can then be converted into the PWV by a conversion factor (Bevis et al. 1994). Because the conversion factor is a function of the weighted mean temperature, its accuracy is directly affected by the weighted mean temperature.

The calculation model for the weighted mean temperature T_m using meteorological data proposed by Davis et al. (1985) is:

$$T_m = \frac{\int_h^\infty \frac{e}{T} dh}{\int_h^\infty \frac{e}{T^2} dh} \tag{3}$$

where e is the water vapour pressure; T is the atmospheric temperature; and h is the height above the mean sea level.

Equation (3) shows that temperature and water vapour profiles are used for the T_m calculation, which can be obtained from radiosonde, RO and Interim European Centre for Medium-Range Weather Forecasts (ECMWF) Re-Analysis (ERA-Interim) products. By discretizing the integral in Equation (3), the following equation is obtained (Chen et al., 2014; Yao et al., 2013):

$$T_m = \frac{\sum_{i=0}^{i=n-1} \left(\frac{e_i}{T_i} + \frac{e_{i+1}}{T_{i+1}}\right)(h_{i+1} - h_i)}{\sum_{i=0}^{i=n-1} \left(\frac{e_i}{T_i^2} + \frac{e_{i+1}}{T_{i+1}^2}\right)(h_{i+1} - h_i)} \tag{4}$$

where e_i indicates the water vapour pressure of the ith layer of the radiosonde data; T_i is the temperature of the ith layer of the radiosonde data; h_i is the height of the ith layer of the radiosonde data; and n is the number of the layer of the radiosonde data. Water vapour pressure usually varies exponentially with height. Therefore, the use of linear discretization in Equation (4) would induce a larger error for T_m. Thus, a new method to mitigate the effects of linear discretization was developed. Vertical change between water vapour pressure, pressure and temperature can be approximately expressed as (Saastamoinen, 1972):

$$\left(\frac{e}{e_s}\right) = \left(\frac{P}{P_s}\right)^{\gamma} \tag{5}$$

$$\left(\frac{P}{P_s}\right) = \left(\frac{T}{T_s}\right)^{\frac{-g_s}{\beta \cdot R_d}} \tag{6}$$

$$T = T_s + \beta(h - h_s) \tag{7}$$

where P denotes atmospheric pressure; e_s, P_s and T_s are the water vapour pressure, pressure and temperature at the surface, respectively; γ is defined as the mixing ratio of the atmosphere; h_s is the height of the surface; g_s is gravity acceleration; R_d is the specific gas constant for dry air; and β is the temperature lapse rate.

According to Equations (5) to (7), one obtains:

$$\frac{e}{T} = \frac{e_s}{T_s} \cdot \left(\frac{T}{T_s}\right)^{\frac{-\gamma g_s}{\beta \cdot R_d} - 1} \tag{8}$$

The integral of (e/T) for a given interval $[h_1,h_2]$ is expressed as:

$$\int_{h_1}^{h_2} \frac{e}{T} dh = \int_{h_1}^{h_2} \frac{e_1}{T_1} \cdot \left(\frac{T}{T_1}\right)^{E^{1,2}-1} dh = \frac{e_1}{E^{1,2} \cdot \beta^{1,2}} \left(\left(\frac{T_2}{T_1}\right)^{E^{1,2}} - 1\right) \tag{9}$$

where $E^{1,2} = \frac{lne_2 - lne_1}{lnT_2 - lnT_1}$; $g_1 = 9.784 \cdot (1 - 0.0026 \cdot cos(2\varphi) - 2.8 \times 10^{-7} \cdot h_1)$, $\beta^{1,2} = \frac{T_2 - T_1}{h_2 - h_1}$; and φ is the latitude.

According to Equations (8) and (9), the integral of (e/T^2) for the interval $[h_1,h_2]$ is expressed as:

$$\int_{h_1}^{h_2} \frac{e}{T^2} dh = \int_{h_1}^{h_2} \frac{1}{T} \cdot \frac{e_1}{T_1} \cdot \left(\frac{T}{T_1}\right)^{E^{1,2}-1} dh = \frac{e_1}{(E^{1,2}-1) \cdot T_1 \cdot \beta^{1,2}} \left(\left(\frac{T_2}{T_1}\right)^{E^{1,2}-1} - 1\right) \tag{10}$$

Considering Equations (9) and (10), Equation (3) can be discretized as:

$$T_m = \frac{\sum_{i=0}^{i=n-1} \frac{e_i}{E^{i,i+1}\cdot\beta^{i,i+1}} \left(\left(\frac{T_{i+1}}{T_i}\right)^{E^{i,i+1}} - 1 \right)}{\sum_{i=0}^{i=n-1} \frac{e_i}{\left(E^{i,i+1}-1\right)\cdot T_i\cdot\beta^{i,i+1}} \left(\left(\frac{T_{i+1}}{T_i}\right)^{E^{i,i+1}-1} - 1 \right)} \quad (11)$$

Equation (11) takes account for the exponential variations of water vapour pressure and linear changes of temperature with height. The advantage of Equation (11) will be verified in Sections 3.3 and 3.4.

3 | REGIONAL T_m MODEL

3.1 | Establishing the T_m model

The regional T_m model RT_m can be constructed by establishing the relationships for T_m with the T_s, H and D variables based on radiosonde and COSMIC historical data.

The model between the T_m and date (D) can then be estimated by:

$$T_m(D) = a + b\cdot\cos\left(2\pi\frac{(D-28)}{365.25}\right) + c\cdot\sin\left(2\pi\frac{(D-28)}{365.25}\right) \quad (12)$$

where a, b and c are parameters of the model that can be determined by radiosonde and COSMIC profile historical data.

In addition, the models for the T_m and T_s and for the T_m and height H can be expressed by the quadratic functions:

$$T_m(T_s) = p_2\cdot T_s^2 + p_1\cdot T_s + p \quad (13)$$

$$T_m(H) = q_2\cdot H^2 + q_1\cdot H + q \quad (14)$$

where p_2, p_1, p, and q_2, q_1 and q are two sets of three parameters of the model which are determined by radiosonde and COSMIC profile historical data.

3.2 | Data collection

The COSMIC occultation is a joint Taiwan/US science mission for weather, climate, space weather and geodetic research, especially in regions with sparse data, including the oceans and near the Poles (Schreiner et al., 2007; Anthes et al., 2008). The Integrated Global Radiosonde Archive (IGRA) consists of radiosonde and pilot balloon observations from more than 2,700 globally distributed stations, and recently data have become available in near-real time. Observations are available at standard and variable pressure levels, fixed- and variable-height wind levels, and the surface and tropopause. The variables include pressure, temperature, geopotential height, relative humidity, dew point depression, wind direction and speed, and elapsed time since launch. Both COSMIC and radiosonde products are important sources for improving global weather forecasting and climate analysis (Kuo et al., 2005; Kishore et al., 2011).

The COSMIC Data Analysis and Archive Center (CDAAC) provides both the real-time and post-processed data products, and they are freely available for public access (www.cosmic.ucar.edu). The post-processed profiles used in the present paper are usually available with six week latency. The COSMIC wetPrf profile is an atmospheric occultation profile of pressure, temperature and moisture information interpolated to 100 m height levels; the COSMIC sonPrf profile offers temperature, pressure and moisture profiles and can also be used for comparison with the wetPrf profile.

The present study collected the radiosonde data from the 45,004th radiosonde station, which is equipped with a Vaisala RS92 sensor. The pressure and temperature measurements of this sensor are accurate within 1 hPa and 0.5°C, respectively, and the total uncertainty in sounding and repeatability by the humidity sensor are $> 5\%$ and 2%, respectively (www.vaisala.com) (UWYO, 2018). Furthermore, the COSMIC RO profiles are collocated in the Hong Kong area that occurred from latitude 22 to 22.8° N and from longitude 113.5 to 114.5° E between 2007 and 2015. Compared with the radiosonde technique, the COSMIC RO is equipped with a compact, low-power and low-cost sensor and it offers a high-accuracy meteorological product with averaged profile temperatures of < 0.1 K (http://www.cosmic.ucar.edu/ro.html). Using the sonPrf profiles as references, quality control of the wetPrf profiles was first performed. A total of 1,484 RO events occurred in or near Hong Kong between 2007 and 2016. The statistical results for < 10 km height are shown in Table 1.

As shown in Table 1, the maximum biases of temperature and water vapour pressure between wetPrf and sonPrf are 7.98 K and 12.39 mbar, respectively, which in

this case will bring in obvious errors when obtaining the T_m. Therefore, it is critical to examine the wetPrf profiles. In addition, the authors tried to assess the number of RO events that reach heights up to 3 km above the surface in Hong Kong. From the statistics, one can see that a total of 1,048 RO events satisfy this condition. Besides, if the differences of temperature and water vapour pressure between wetPrf and sonPrf are > 2.54 K and 3.14 mbar (2σ) < 3 km, the data will be truncated below this height.

3.3 | Accuracy of the new T_m integration method

The T_m can be expressed as a function of temperature T and water vapour pressure e. The calculation model of the T_m is traditionally discretized based on a linear function. The integral of (e/T) for a given interval $[h_1,h_2]$ is then expressed as:

$$\int_{h_1}^{h_2}\frac{e}{T}dh=\int_{h_1}^{h_2}\left(K_1(h-h_1)+\frac{e_1}{T_1}\right)dh =\left(\frac{K_1(h_2-h_1)}{2}+\frac{e_1}{T_1}\right)(h_2-h_1)=\frac{\left(\frac{e_1}{T_1}+\frac{e_2}{T_2}\right)}{2}(h_2-h_1) \tag{15}$$

where $K_1=\frac{\frac{e_2}{T_2}-\frac{e_1}{T_1}}{h_2-h_1}$.

Similarly, the integral of (e/T^2) for the interval $[h_1,h_2]$ is expressed as:

$$\int_{h_1}^{h_2}\frac{e}{T^2}dh=\int_{h_1}^{h_2}\left(K_2(h-h_1)+\frac{e_1}{T_1^2}\right)dh =\left(\frac{K_2(h_2-h_1)}{2}+\frac{e_1}{T_1^2}\right)(h_2-h_1)=\frac{\left(\frac{e_1}{T_1^2}+\frac{e_2}{T_2^2}\right)}{2}(h_2-h_1) \tag{16}$$

where $K_2=\frac{\frac{e_2}{T_2^2}-\frac{e_1}{T_1^2}}{h_2-h_1}$.

The T_m can then be expressed as:

$$T_m=\frac{\sum_{i=0}^{i=n-1}\left(\frac{e_i}{T_i}+\frac{e_{i+1}}{T_{i+1}}\right)(h_{i+1}-h_i)}{\sum_{i=0}^{i=n-1}\left(\frac{e_i}{T_i^2}+\frac{e_{i+1}}{T_{i+1}^2}\right)(h_{i+1}-h_i)} =\frac{\sum_{i=0}^{i=n-1}\left(\frac{k_1^i(h_{i+1}-h_i)}{2}+\frac{e_i}{T_i}\right)(h_{i+1}-h_i)}{\sum_{i=0}^{i=n-1}\left(\frac{k_2^i(h_{i+1}-h_i)}{2}+\frac{e_i}{T_i^2}\right)(h_{i+1}-h_i)} \tag{17}$$

To evaluate the accuracy of the traditional T_m model, Equation (17) is first differentiated:

$$d_{T_m}=\frac{\sum_{i=0}^{i=n-1}(h_{i+1}-h_i)d\left(\frac{e_i}{T_i}\right)}{\sum_{i=0}^{i=n-1}\left[\frac{k_2^i(h_{i+1}-h_i)}{2}+\frac{e_i}{T_i^2}\right](h_{i+1}-h_i)} -\frac{\sum_{i=0}^{i=n-1}\left[\frac{k_1^i(h_{i+1}-h_i)}{2}+\frac{e_i}{T_i}\right](h_{i+1}-h_i)^2d\left(\frac{e_i}{T_i^2}\right)}{\left\{\sum_{i=0}^{i=n-1}\left[\frac{k_2^i(h_{i+1}-h_i)}{2}+\frac{e_i}{T_i^2}\right](h_{i+1}-h_i)\right\}^2} \tag{18}$$

$$d\left(\frac{e_i}{T_i}\right)=\frac{d_{e_i}}{T_i}-\frac{e_i}{T_i^2}d_{T_i} \tag{19}$$

$$d\left(\frac{e_i}{T_i^2}\right)=\frac{d_{e_i}}{T_i^2}-\frac{2\cdot e_i}{T_i^3}d_{T_i} \tag{20}$$

According to Equations (18) to (20), one obtains:

$$\begin{aligned}d_{T_m}=&\frac{\sum_{i=0}^{i=n-1}\left[\frac{h_{i+1}-h_i}{T_i}\right]d_{e_i}}{\sum_{i=0}^{i=n-1}\left[\frac{K_2^ih_{i+1}-h_i}{2}+\frac{e_i}{T_i^2}\right]h_{i+1}-h_i}\\ &-\frac{\sum_{i=0}^{i=n-1}\frac{h_{i+1}-h_i^2}{T_i^2}\left[\frac{K_1^ih_{i+1}-h_i}{2}+\frac{e_i}{T_i}\right]d_{e_i}}{\sum_{i=0}^{i=n-1}\left\{\left[\frac{K_2^ih_{i+1}-h_i}{2}+\frac{e_i}{T_i^2}\right]h_{i+1}-h_i\right\}^2}\\ &-\frac{\sum_{i=0}^{i=n-1}\left[\frac{e_ih_{i+1}-h_i}{T_i^2}\right]d_{T_i}}{\sum_{i=0}^{i=n-1}\left[\frac{K_2^ih_{i+1}-h_i}{2}+\frac{e_i}{T_i^2}\right]h_{i+1}-h_i}\\ &+\frac{\sum_{i=0}^{i=n-1}\frac{2e_ih_{i+1}-h_i^2}{T_i^3}\left[\frac{K_1^ih_{i+1}-h_i}{2}+\frac{e_i}{T_i}\right]d_{T_i}}{\sum_{i=0}^{i=n-1}\left\{\left[\frac{K_2^ih_{i+1}-h_i}{2}+\frac{e_i}{T_i^2}\right]h_{i+1}-h_i\right\}^2}\end{aligned} \tag{21}$$

TABLE 1 Statistical results of the differences between wetPrf and sonPrf at < 10 km

	Maximum	Minimum	Mean	RMS
Temperature (T)	7.98	0.006	0.33	1.27
H_2O pressure (mbar)	12.39	0.001	0.39	1.57

Note: H_2O pressure: water vapour pressure; Maximum: maximum deviation between wetPrf and sonPrf; Minimum: minimum deviation between wetPrf and sonPrf; Mean: mean deviation between wetPrf and sonPrf; RMS: root mean square of the deviation between wetPrf and sonPrf.

$$d_{T_m}=\frac{\sum_{i=0}^{i=n-1}\left[\left(\frac{T_{i+1}}{T_i}\right)^{E^{i,i+1}}-1\right]d_{e_i}}{\sum_{i=0}^{i=n-1}\frac{e_i}{(E^{i,i+1}-1)\cdot T_i\cdot\beta^{i,i+1}}\left[\left(\frac{T_{i+1}}{T_i}\right)^{E^{i,i+1}-1}-1\right]}-\frac{\sum_{i=0}^{i=n-1}\frac{e_i}{E^{i,i+1}\cdot\beta^{i,i+1}}\left[\left(\frac{T_{i+1}}{T_i}\right)^{E^{i,i+1}}-1\right]\cdot\sum_{i=0}^{i=n-1}\frac{\left[\left(\frac{T_{i+1}}{T_i}\right)^{E^{i,i+1}}-1\right]}{(E^{i,i+1}-1)\cdot T_i\cdot\beta^{i,i+1}}\cdot d_{e_i}}{\sum_{i=0}^{i=n-1}\left\{\frac{e_i}{(E^{i,i+1}-1)\cdot T_i\cdot\beta^{i,i+1}}\left[\left(\frac{T_{i+1}}{T_i}\right)^{E^{i,i+1}-1}-1\right]\right\}^2}$$
$$-\frac{\sum_{i=0}^{i=n-1}\frac{e_i}{T_i^2}\cdot\left(\frac{T_{i+1}}{T_i}\right)^{E^{i,i+1}-1}(h_{i+1}-h_i)d_{T_i}}{\sum_{i=0}^{i=n-1}\frac{e_i}{(E^{i,i+1}-1)\cdot T_i\cdot\beta^{i,i+1}}\left[\left(\frac{T_{i+1}}{T_i}\right)^{E^{i,i+1}-1}-1\right]}-\sum_{i=0}^{i=n-1}\frac{e_i}{E^{i,i+1}\cdot\beta^{i,i+1}}\left[\left(\frac{T_{i+1}}{T_i}\right)^{E^{i,i+1}}-1\right]$$
$$\frac{\sum_{i=0}^{i=n-1}\frac{e_i}{(E^{i,i+1}-1)\cdot\beta^{i,i+1}}\cdot\left[\frac{\left((E^{i,i+1}-1)\cdot(T_{i+1})^{E^{i,i+1}-2}\right)}{(T_i)^{E^{i,i+1}}}-\frac{\left(E^{i,i+1}\cdot(T_{i+1})^{E^{i,i+1}-1}\right)}{(T_i)^{E^{i,i+1}+1}}+\frac{1}{T_i^2}\right]d_{T_i}}{\sum_{i=0}^{i=n-1}\left\{\frac{e_i}{(E^{i,i+1}-1)\cdot T_i\cdot\beta^{i,i+1}}\left[\left(\frac{T_{i+1}}{T_i}\right)^{E^{i,i+1}-1}-1\right]\right\}^2} \tag{22}$$

To evaluate the accuracy of the optimized T_m model, Equation (11) can be differentiated as:

The water vapour partial pressure e can be derived as follows

$$e_i=6.1121\left(1.0007+3.46\times10^{-6}\cdot P_i\right)\cdot RH_i\cdot exp\left\{\frac{[18.729-(T_i-273.15)/227.3](T_i-273.15)}{T_i-15.28}\right\} \tag{23}$$

where RH is the relative humidity. Equation (23) can then be differentiated as:

$$d_{e_i}=Q_1^i\cdot d_{P_i}+Q_2^i\cdot d_{T_i}+Q_3^i\cdot d_{RH_i} \tag{24}$$

where Q_1^i, Q_2^i and Q_3^i represent:

$$Q_1^i=21.147899\times10^{-6}\cdot \mathrm{RH}_i\cdot exp^{\theta_i}$$

$$Q_2^i=6.1121\cdot RH_i\left(1.0007+3.46\times10^{-6}\cdot P_i\right)exp^{\theta_i}\cdot\frac{18.729-2(T_i-273.15)/227.3-\theta_i}{T_i-15.28}$$

$$Q_3^i=6.1121\cdot\left(1.0007+3.46\times10^{-6}\cdot P_i\right)\cdot exp^{\theta_i}$$

$$\theta_i=\frac{[18.729-(T_i-273.15)/227.3](T_i-273.15)}{T_i-15.28}$$

Substituting Equation (24) into Equations (21) and (22), respectively, and with the assumption that the measurements of pressure, temperature and relative humidity are uncorrelated, one can derive the uncertainty of T_m, denoted as $\delta_{\Delta T_m}$, with the error propagation law:

$$\delta_{\Delta T_m}^{Trad}=\sqrt{A_1^2\cdot\delta_P^2+A_2^2\cdot\delta_T^2+A_3^2\cdot\delta_{RH}^2} \tag{25}$$

$$\delta_{\Delta T_m}^{New}=\sqrt{B_1^2\cdot\delta_P^2+B_2^2\cdot\delta_T^2+B_3^2\cdot\delta_{RH}^2} \tag{26}$$

where δ_P, δ_T and δ_{RH} are the uncertainties of the total pressure, temperature and relative humidity measurements, respectively. In addition, the co-efficients A_1, A_2 and A_3, and B_1, B_2 and B_3 are defined as:

$$A_1=\frac{\sum_{i=0}^{i=n-1}\left\{\left[\frac{(h_{i+1}-h_i)}{T_i}\right]Y-Z\right\}Q_1^i}{\sum_{i=0}^{i=n-1}Y^2} \tag{27}$$

$$A_2=\frac{\sum_{i=0}^{i=n-1}\left\{\left[\frac{(h_{i+1}-h_i)}{T_i}\right]Y-Z\right\}Q_{2-}^i\left[\frac{e_i(h_{i+1}-h_i)}{T_i^2}\right]\cdot Y+X}{\sum_{i=0}^{i=n-1}Y^2} \tag{28}$$

$$A_3=\frac{\sum_{i=0}^{i=n-1}\left\{\left[\frac{(h_{i+1}-h_i)}{T_i}\right]Y-Z\right\}Q_3^i}{\sum_{i=0}^{i=n-1}Y^2} \tag{29}$$

$$Y=\left[\frac{K_2^i(h_{i+1}-h_i)}{2}+\frac{e_i}{T_i^2}\right](h_{i+1}-h_i) \tag{30}$$

$$Z=\frac{(h_{i+1}-h_i)^2}{T_i^2}\left[\frac{K_1^i(h_{i+1}-h_i)}{2}+\frac{e_i}{T_i}\right] \tag{31}$$

$$X = \frac{2e_i(h_{i+1}-h_i)^2}{T_i^3}\left[\frac{K_1^i(h_{i+1}-h_i)}{2}+\frac{e_i}{T_i}\right] \tag{32}$$

$$B_1 = \frac{\sum_{i=0}^{i=n-1}\left\{D\left[\frac{T_{i+1}}{T_i}E^{i,i+1}-1\right]-F\cdot\frac{\left[\frac{T_{i+1}}{T_i}E^{i,i+1}-1\right]}{E^{i,i+1}-1\cdot T_i\cdot\beta^{i,i+1}}\right\}Q_1^i}{\sum_{i=0}^{i=n-1}D^2} \tag{33}$$

$$B_2 = \frac{\sum_{i=0}^{i=n-1}\left\{D\left[\left(\frac{T_{i+1}}{T_i}\right)^{E^{i,i+1}}-1\right]-F\cdot\frac{\left[\left(\frac{T_{i+1}}{T_i}\right)^{E^{i,i+1}}-1\right]}{(E^{i,i+1}-1)\cdot T_i\cdot\beta^{i,i+1}}-D\cdot G-F\cdot H\right\}Q_2^i}{\sum_{i=0}^{i=n-1}D^2} \tag{34}$$

$$B_3 = \frac{\sum_{i=0}^{i=n-1}\left\{D\left[\frac{T_{i+1}}{T_i}E^{i,i+1}-1\right]-F\cdot\frac{\left[\frac{T_{i+1}}{T_i}E^{i,i+1}-1\right]}{E^{i,i+1}-1\cdot T_i\cdot\beta^{i,i+1}}\right\}Q_3^i}{\sum_{i=0}^{i=n-1}D^2} \tag{35}$$

$$D = \frac{e_i}{\left(E^{i,i+1}-1\right)\cdot T_i\cdot\beta^{i,i+1}}\left[\left(\frac{T_{i+1}}{T_i}\right)^{E^{i,i+1}-1}-1\right] \tag{36}$$

$$F = \frac{e_i}{E^{i,i+1}\cdot\beta^{i,i+1}}\left[\left(\frac{T_{i+1}}{T_i}\right)^{E^{i,i+1}}-1\right] \tag{37}$$

$$G = \frac{e_i}{T_i^2}\cdot\left(\frac{T_{i+1}}{T_i}\right)^{E^{i,i+1}-1}(h_{i+1}-h_i) \tag{38}$$

$$H = \frac{e_i}{(E^{i,i+1}-1)\cdot\beta^{i,i+1}}\cdot\left[\frac{\left((E^{i,i+1}-1)\cdot(T_{i+1})^{E^{i,i+1}-2}\right)}{(T_i)^{E^{i,i+1}}}-\frac{\left(E^{i,i+1}\cdot(T_{i+1})^{E^{i,i+1}-1}\right)}{(T_i)^{E^{i,i+1}+1}}+\frac{1}{T_i^2}\right] \tag{39}$$

Using the nine year radiosonde data of the 45,004th station, the empirical values of A_1, A_2 and A_3, and B_1, B_2 and B_3 were computed. However, only their maximum, minimum and means are given in Table 2. The specified pressure, temperature and RH accuracies for radiosonde instrumentation are $\delta_P = 1\ hPa$, $\delta_T = 0.5$ K and $\delta_{RH} = 0.05$, respectively. By substituting these values and those in Table 2 into Equations (25) and (26), the corresponding $\delta_{\Delta T_m}^{Trad}$ and $\delta_{\Delta T_m}^{New}$ are derived and given in the last two rows of Table 2. The results show that both A_1 and B_1 are very small, which verifies that the effect of P on T_m is negligible. In addition, the mean accuracies of $\delta_{\Delta T_m}^{Trad}$ and $\delta_{\Delta T_m}^{New}$ derived from the radiosonde are 3.67 and 2.29 K, respectively.

TABLE 2 Uncertainties estimated from the radiosonde measurements

	Maximum	Minimum	Mean
A_1	6.2128×10^{-6}	1.9673×10^{-6}	4.0153×10^{-6}
A_2	−13.2120	−2.3101	−7.3225
A_3	3.7352	0.7448	1.3048
B_1	4.0924×10^{-6}	1.1650×10^{-6}	2.9240×10^{-6}
B_2	−9.1214	−1.4322	−4.5702
B_3	2.1758	0.5502	1.0877
$\delta_{\Delta T_m}^{Trad}$ (K)	6.6082	1.1557	3.6618
$\delta_{\Delta T_m}^{New}$ (K)	4.5620	0.7166	2.2857

3.4 | Verification of the new T_m integration method

The COSMIC wetPrf profile contains atmospheric occultation profiles and moisture information. Gridded analysis and/or short-term forecasting are used to separate the pressure, temperature and moisture that contribute to refractivity, and this profile is interpolated to 100 m heights. To validate the advantages of the new integration method, the radiosonde products and wetPrf profiles were first tested with different sampling intervals. The T_m that derived from the radiosonde data based on Equations (4) and (11) are denoted RadTrad and RadNew, respectively. The T_m values obtained using radiosonde data every two sampling intervals based on Equations (4) and (11) are denoted RadTrad2 and RadNew2. In addition, the T_m values derived from wetPrf profiles based on Equations (4) and (11) are denoted COSTrad and COSNew. The T_m values obtained using wetPrf profiles with different sampling intervals based on Equations (4) and (11) are denoted RadTradD and RadNewD. Using the nine year radiosonde data from the 45,004th station, the empirical values for RadTrad, RadNew, RadTrad2 and RadNew2 were computed. The wetPrf profiles from in or near Hong Kong from 2007 to 2016 are used to obtain the COSTrad, COSNew, COSTradD and COSNewD. The statistical results are shown in Tables 3 and 4.

As shown in Tables 3 and 4, the maximum deviation between the RadNew and RadNew2 is −11.12 K, and the maximum bias between the RadTrad and RadTrad2 is −16.88 K. The maximum deviation between the COSNew and COSNewD is 11.41 K, and the maximum deviation between the COSTrad and COSTradD is 11.98 K. In

TABLE 3 Statistical results for the T_m with different sampling based on radiosonde data (K)

	RadNew – RadNew2				RadTrad – RadTrad2			
Year	Maximum	Minimum	Mean	RMS	Maximum	Minimum	Mean	RMS
2007	5.91	−8.01	0.07	2.10	7.08	−11.48	0.68	2.52
2008	5.25	−7.87	−0.03	2.03	7.95	−11.59	0.82	2.47
2009	5.76	−9.51	0.09	2.02	8.71	−12.09	0.89	2.65
2010	5.91	−12.91	−0.13	2.08	7.56	−11.49	0.93	2.41
2011	6.57	−11.12	0.08	2.21	8.11	−12.67	0.85	2.71
2012	5.45	−9.95	−0.05	2.01	7.86	−12.15	0.71	2.51
2013	6.84	−9.22	−0.20	2.14	7.27	−11.23	0.83	2.65
2014	6.50	−9.12	0.09	1.95	9.08	−10.91	0.66	2.45
2015	6.33	−8.55	0.02	1.99	9.41	−12.75	0.74	2.52
2016	5.33	−8.02	0.08	2.11	7.01	−16.88	0.75	2.77

Note: RadTrad and RadNew: the T_m derived from the radiosonde data based on Equations (4) and (11), respectively; RadTrad2 and RadNew2: the T_m obtained using radiosonde data every two sampling intervals based on Equations (4) and (11), respectively.
Abbreviation: RMS: root mean square.

TABLE 4 Statistical results for the T_m with different sampling based on wetPrf profiles (K)

	COSNew – COSNewD				COSTrad – COSTradD			
Sampling	Maximum	Minimum	Mean	RMS	Maximum	Minimum	Mean	RMS
0.5 km	3.34	−1.24	0.82	0.97	3.69	−1.91	0.98	1.12
1.0 km	8.91	−9.01	1.01	3.29	9.92	−9.97	1.12	3.52
1.5 km	11. 41	−11.03	1.73	3.98	11.98	−11.53	1.81	4.30

Note: COSTrad and COSNew: the T_m derived from wetPrf profiles based on Equations (4) and (11), respectively; RadTradD and RadNewD: the T_m obtained using wetPrf profiles with different sampling intervals based on Equations (4) and (11), respectively.
Abbreviation: RMS: root mean squares.

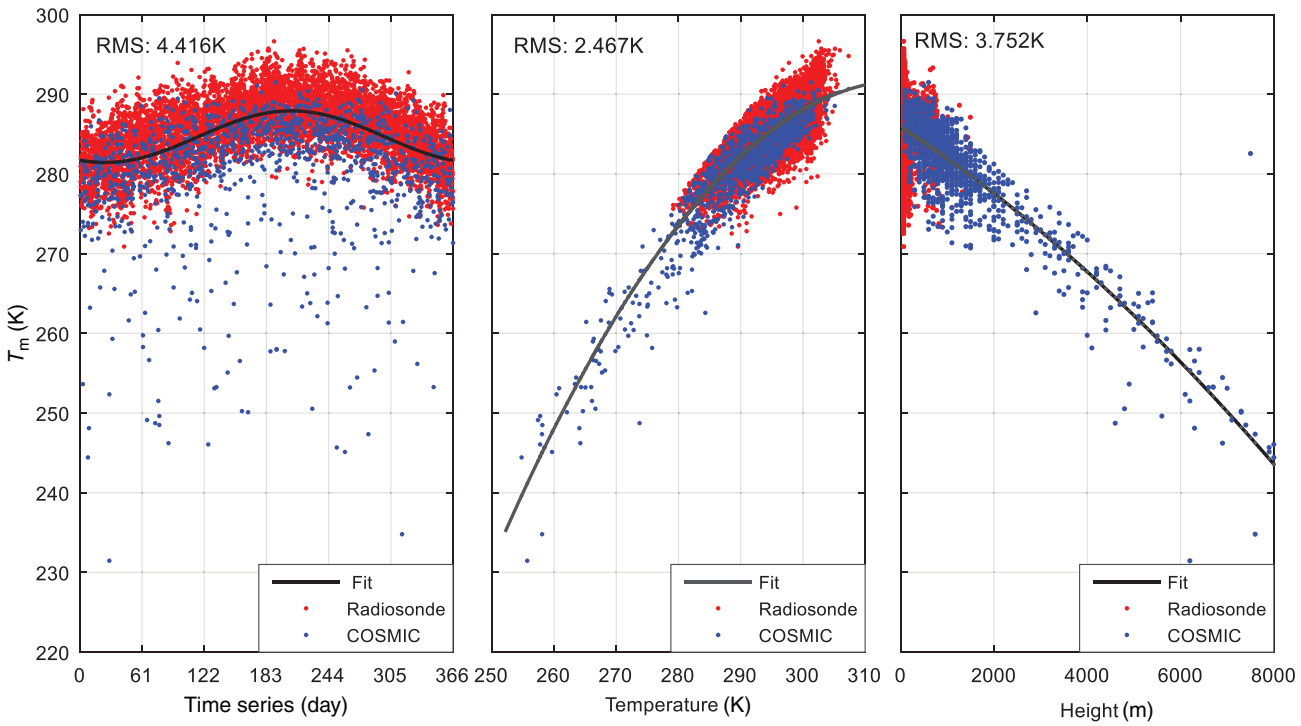

FIGURE 1 Relationships between the T_m and time, the T_m and surface temperature, and the T_m and height. Fit: fit function; radiosonde: the T_m derived from radiosonde products using the new method; and COSMIC: the T_m derived from wetPrf profiles using the new method

addition, the root mean square (RMS) of difference between the RadNew and RadNew2 is > 2.1 K, and the RMS of deviation between the RadTrad and RadTrad2 is 2.6 K. The RMS of difference between the COSNew and COSNewD is > 2.75 K, and the RMS of the deviation between the COSTrad and COSTradD is 2.98 K. From the results of the statistics, it can be seen that the accuracies of the RadNew2, RadTrad2, COSNewD and COSTradD are worse than that of the RadNew, RadTrad, COSNew and COSTrad, respectively. The differences between the RadNew and RadNew2 and COSNew and COSNewD are smaller than the differences between the RadTrad and RadTrad2, and COSTrad and COSTradD. Compared with RADTrad, the quality of RADTrad2 is decreased by 2.57 K, and compared with RADNew, the quality of RADNew2 is decreased by 2.06 K. In addition, compared with the COSTrad, the accuracy of the COSTradD is reduced by 2.98 K, and compared with the COSNew, the accuracy of the COSNewD is reduced by 2.74 K.

3.5 | Establishing the relationship between the T_m and T_s, D and H

One need not consider the differences in latitude and longitude because the COSMIC product near or inside Hong Kong and the radiosonde data from the 45,004th station were put together to match with ascending order in time. The relationship between the T_m and time is established based on Equation (12) (left in Figure 1). The connections between the T_m and surface temperature and height were then built using Equations (13) and (14), respectively (middle and right in Figure 1, respectively).

Figure 1 illustrates that the mathematical models can establish well the relationships between the T_m and time, surface temperature and height. The RMSs of the goodness of fit are 4.416, 2.467 and 3.752 K, respectively. In addition, the relationships between the T_m and time and height are established by joining Equations (12) and (14), respectively (left in Figure 2). The relationships between the T_m and time and height are built by combining Equations (13) and (14), respectively (middle in Figure 2). The relevance between the T_m and time and height are set up by combining Equations (12) and (13), respectively (right in Figure 2).

Figure 2 indicates that the T_m model that accounts for the effects of two parameters is better than those that consider the effects of only one parameter. The RMSs of goodness of fit are 2.965, 2.362 and 2.347 K between the T_m and time and height, T_m and surface temperature and height, and T_m and time and surface temperature, respectively.

4 | VALIDATION OF THE RESULTS AND DISCUSSION

The results were verified by the same data sets as described in Section 3.1. The COSMIC wetPrf profiles that occurred in or near Hong Kong and from the 45,005th radiosonde data from January 1 to October 31, 2016, were used to evaluate the accuracy of the T_m models.

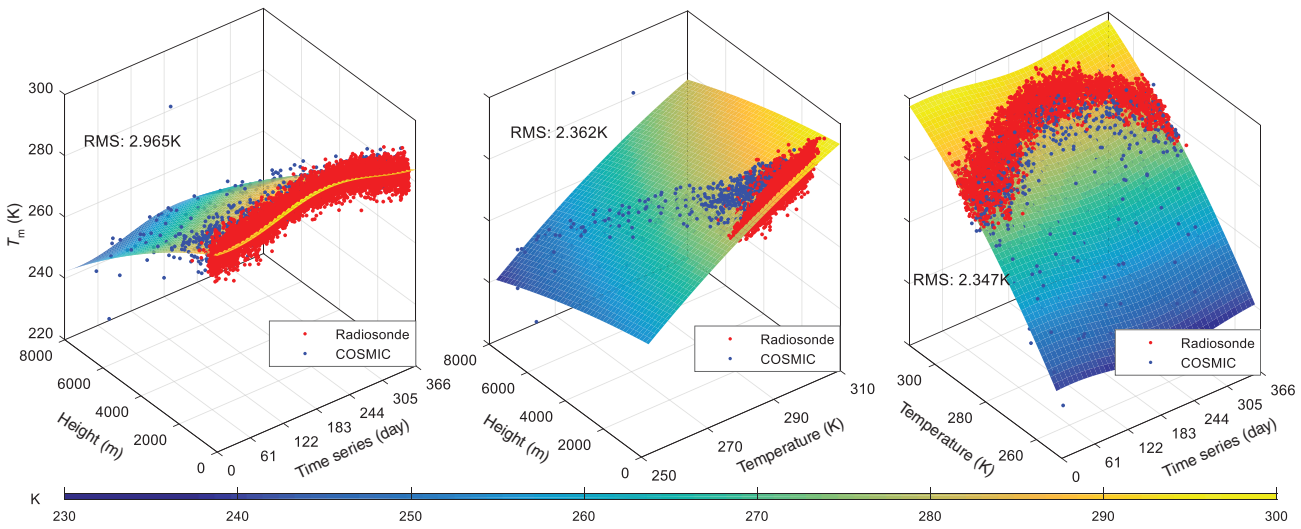

FIGURE 2 Relationships between the T_m and time and height, the T_m and surface temperature and height, and the T_m and time and surface temperature. Radiosonde: the T_m derived from radiosonde products using the new method; and COSMIC: the T_m derived from wetPrf profiles using the new method

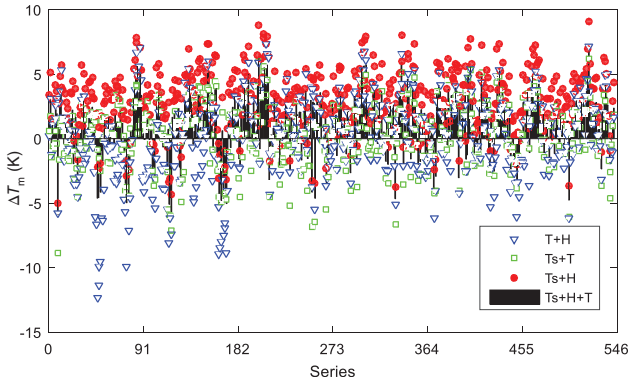

FIGURE 3 Comparisons of the T_m obtained from four models and radiosonde from January 1 to October 31, 2016. T + H: the model is established using time and height; Ts + T: the model is established based on surface temperature and time; Ts + H: the model is established based on surface temperature and height; and Ts + H + T: the model is established based on surface temperature, height and time

TABLE 5 Statistical results for model- and radiosonde-derived T_m (K)

	T_m			
	Maximum	**Minimum**	**Mean**	**RMS**
Bevis	5.01	−8.89	−2.69	3.37
Wang	8.68	−4.91	1.03	2.32
GT_m_III	9.41	−6.62	3.77	3.96
GT_m_N	11.04	−7.36	4.25	4.38
$T_s + H$	6.71	−11.97	0.04	2.76
$T_s + D$	5.45	−5.90	0.31	1.84
$D + H$	7.94	−4.08	0.18	3.42
$T_s + H + D$	6.45	−5.05	0.19	2.24

Abbreviation: RMS: root mean squares.

4.1 | Comparison of the model- and radiosonde-derived results

In the present study, model 1 is defined by Equation (12), model 2 is defined by Equation (13), and model 3 is defined by Equation (14). The T_m results were obtained from models 1 + 3 ($D + H$), models 1 + 2 ($D + T_s$), models 2 + 3 ($T_s + H$), and models 1 + 2 + 3 ($D + T_s + H$) based on radiosonde data, respectively. Figure 3 shows the comparison results using the T_m derived from radiosonde products based on Equation (11) as references.

Compared with the T_m obtained from models 1 + 2 ($D + T_s$), models 2 + 3 ($T_s + H$), and models 1 + 2 + 3 ($D + T_s + H$) the results derived from models 1 + 3 ($D + H$) are relatively poor because this model does not consider the effects of surface temperature. Because the $T_s + H + D$ model considers surface temperature, height and time, it is the most accurate. Several traditional global weighted mean temperature models, such as GT_m_III (Yao et al., 2014), GT_m_N (Chen et al., 2014), Bevis models and regional model (Wang et al., 2011) suitable for Hong Kong regions have been developed. To evaluate these new models and the traditional models, the statistical results between model- and radiosonde-derived atmospheric weighted average temperatures based on Equation (11) are provided using 305 day data sets from January 1 to October 31, 2016, in Hong Kong (Table 5).

Table 5 provides the maximum, minimum, mean and RMS of the differences between the T_m derived by the models and that derived by radiosonde data. The RMS of deviation between the GT_m_N model- and radiosonde-derived T_m is 4.38 K, which is bigger than the other models, and the maximum of the deviation between the GT_m_N model- and radiosonde-derived T_m is 11.04 K, which is worse than the other models. In addition, the RMS and maximum of the deviation between the $T_s + D$ model- and radiosonde-derived T_m are 5.45 and 1.84 K, which is better than the other models. In terms of the statistical results, it can be seen that the $T_s + H + D$ and $T_s + D$ models are more accurate than the other models. The GT_m_III and GT_m_N do not consider the surface meteorology elements, so their results are worse than those of the Bevis and the Wang models. In addition, compared with the Bevis model, the RMS statistical results confirm that the accuracy of the T_m derived by the $T_s + D$ model was improved by 45.40%, over those of the Bevis model. Compared with the Wang model, the RMS statistical results confirm that the accuracy of the T_m derived by the $T_s + D$ model was improved by 20.69%, over those of the Wang model. Therefore, the $T_s + D$ model is suggested to estimate the T_m in Hong Kong.

4.2 | Comparison of the model- and COSMIC-derived results

The T_m results were derived using models 1 + 3 ($D + H$), models 1 + 2 ($D + T_s$), models 2 + 3 ($T_s + H$), and models 1 + 2 + 3 ($D + T_s + H$) based on the wetPrf profiles, respectively. Figure 4 shows the comparison results using the T_m values derived from the wetPrf data and based on Equation (11) as references.

By comparing the results of wetPrf profiles in Figure 4, it was found that the $T_s + H + D$ model is better than the other models. The $D + H$ model is the least accurate because it does not account for meteorological elements. A total of 31 COSMIC occultation events

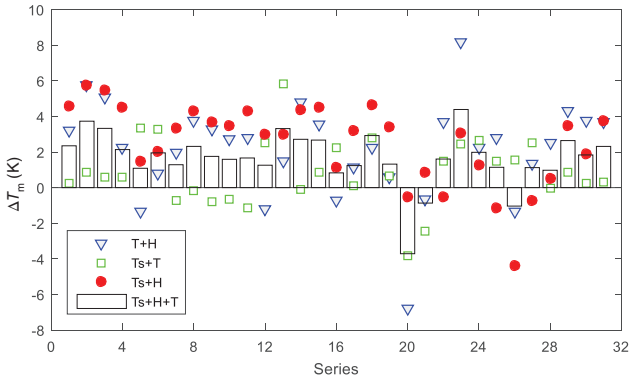

FIGURE 4 Comparisons of the T_m obtained from four models and wetPrf from January 1 to October 31, 2016 in the Hong Kong region. T + H: the model is established using time and height; Ts + T: the model is established based on surface temperature and time; Ts + H: the model is established based on surface temperature and height; and Ts + H + T: the model is established combining surface temperature, height and time

TABLE 6 Statistical results for model- and wetPrf-derived T_m (K)

	T_m		
	Maximum	**Minimum**	**Mean**
Bevis	−1.16	−7.57	−3.97
Wang	5.52	−3.74	1.41
GT_m_III	8.34	−4.62	3.31
GT_m_N	9.02	−5.46	3.53
$T_s + H$	6.01	2.43	2.78
$T_s + D$	4.35	−0.03	1.91
$D + H$	6.81	1.24	3.19
$T_s + H + D$	5.52	1.09	2.65

occurred in or near Hong Kong during the period January 1–October 31, 2016. Their results were used to compare the results of the T_m derived from the four models and with that derived from the traditional model based on Equation (11), respectively (Table 6).

Table 6 provides the maximum, minimum, mean and RMS of the differences between the T_m derived by the models and that derived by the wetPrf. The maximum and RMS of the differences between GT_m_N model- and wetPrf-derived T_m are 9.02 and 3.53 K, which is bigger than the other models. The maximum and RMS of the deviations between the $T_s + D$ model- and wetPrf-derived T_m are 4.35 and 1.91 K, respectively, which is smaller than the other models. According to the statistical results, it can be seen that the $T_s + H + D$ and $T_s + D$ models are more accurate than the other two models. In addition, compared with the Bevis model, the RMS statistical results confirm that the T_m derived from the $T_s + D$ model was improved by 34.75% over those derived from the Bevis model. Compared with the Wang model, the RMS statistical results confirm that the T_m derived from the $T_s + D$ model was improved by 4.94% over those derived from the Wang model. Considering its preference, it can be concluded that the $T_s + D$ model is the optical model for the Hong Kong region.

5 | CONCLUSIONS

The regional atmospheric weighted temperature model was established by combining radiosonde and Constellation Observation System for Meteorology Ionosphere and Climate (COSMIC) radio occultation (RO) historical data. The atmospheric weighted mean temperature (T_m) is traditionally estimated based on Equation (4) with radiosonde and COSMIC historical data; however, when the vertical resolution of these products is poor and/or an inverse layer phenomenon exists, the calculation of the T_m with the traditional method will result in a large error. Therefore, a new function model was proposed that integrates the vertical change of the water vapour and the linearity of the temperature into Equation (3). By differentiating the traditional T_m integral model and new T_m integral model, the mean accuracies of the $\delta_{\Delta T_m}^{Trad}$ and $\delta_{\Delta T_m}^{New}$ derived from the radiosonde are >3.67 and 2.29 K, respectively. According to the law of the T_m variation with surface temperature, time and height, the $T_s + D$, $T_s + H$, $D + H$, and $T_s + D + H$ models (where T_s is surface temperature, D is date and H is height) were then built to estimate the T_m. The wetPrf profiles collocated in the Hong Kong region and the products of the 45,004th radiosonde station from January 1 to October 31, 2016, were used to evaluate the accuracy of the region T_m models. Using radiosonde products as references, compared with the Bevis model, the root mean square (RMS) statistical result confirms that the accuracy of the T_m from the $T_s + D$ model was improved by 45.40% over those from the Bevis model. Compared with the Wang model, the RMS statistical results confirm that the T_m derived from the $T_s + D$ model was improved by 20.69% over those of the Wang model. Using the COSMIC products as references, compared with the Bevis model, the RMS statistical results confirm that the T_m derived from the $T_s + D$ model was improved by 34.75% over those of the Bevis model. Compared with the Wang model, the RMS statistical results confirm that the T_m derived from the $T_s + D$ model was improved by 4.94% over those of the Wang model. The parameters of these new modes can be derived using radiosonde and COSMIC historical

data. In terms of the statistical results, the quality of the $T_s + D$ model is better than that of the other new models; therefore, it is suggested that the $T_s + D$ model be used to obtain the T_m in Hong Kong in the present study. The new T_m model with three parameters is based on equal weights to obtain the T_m in this test. Future research will investigate how to choose the best weight of the three parameters to derive a more accurate T_m.

ACKNOWLEDGEMENTS

The 45004 Kings Park radiosonde observations (UWYO, 2018) can be downloaded at http://weather.uwyo.edu/upperair/sounding.html. In addition, the Constellation Observing System for Meteorology, Ionosphere and Climate-1 program (CDAAC, 2018) offers the COSMIC radio occultation data (wetPrf), which can be freely obtained from http: //cosmic-io.cosmic.ucar.edu/cdaac/index.html. Financial support from the National Natural Science Foundation of China (grant numbers 41904025, 41974031 and 41905027); Fundamental Research Funds for the Central Universities (grant number 2042019kf0032); the China Postdoctoral Science Foundation (grant number 2019M652706); and Henan Science and Technology Public Relations (grant number 172102310178) are greatly appreciated.

ORCID

Pengfei Xia https://orcid.org/0000-0001-5499-0212
Biyan Chen https://orcid.org/0000-0001-5196-0536

REFERENCES

Alber, C., Ware, R., Rocken, C. and Braun, J. (2000) Obtaining single path phase delays from GPS double differences. *Geophysical Research Letters*, 27, 2661–2664.

Anthes, R.A., et al. (2008) The COSMIC/FORMOSAT-3 mission: early results. *Bulletin of the American Meteorological Society*, 89, 1–21.

Askne, J. and Nordius, H. (1987) Estimation of tropospheric delay for microwaves from surface weather data. *Radio Science*, 22, 379–386.

Bevis, M., Businger, S., Herring, A.T., et al. (1992) GPS meteorology: remote sensing of atmospheric water vapor using the global positioning system. *Journal of Geophysical Research*, 97(D14), 15787–15801.

Bevis, M., Businger, S., Chiswell, S., Herring, T.A., Anthes, R.A., Rochen, C. and Ware, R.H. (1994) GPS Meteorology: mapping zenith wet delays onto precipitable water. *Journal of Applied Meteorology*, 33, 379–386.

Black, H.D. (1978) An easily implemented algorithm for the tropospheric range correction. *Journal of Geophysical Research*, 83 (B4), 1825–1828.

Braun, J., Rocken, C. and Ware, R. (2001) Validation of line-of-sight water vapor measurements with GPS. *Radio Science*, 36, 459–472.

Brettle, M.J. and Galvin, J.F.P. (2003) Back to basics: radiosondes: part 1. The instrument. *Weather*, 58, 336–341.

Chen, P., Yao, W.Q. and Zhu, X.J. (2014) Realization of global empirical model for mapping zenith wet delays onto precipitable water using NCEP re-analysis data. *Geophysical Journal International*, 198, 1748–1757.

COSMIC Data Analysis and Archive Center (CDAAC). (2018) *COSMIC Radio Occultation data*. Available at: http://cosmic-io.cosmic.ucar.edu/cdaac/index.html [Accessed 31st November 2018].

Davis, J.L., Herring, T.A., Shapiro, I.I., Rogers, A.E.E. and Elgered, G. (1985) Geodesy by radio interferometry: effects of atmospheric modeling errors on estimates of baseline length. *Radio Science*, 20, 1593–1607. https://doi.org/10.1029/RS020i006p01593.

Gu, X.P., Wang, C.Y. and Wu, D.X. (2005) Research on the local algorithm for weighted atmospheric temperature used in GPS remote sensing water vapor. *Scientia Meteorologica Sinica*, 25, 79–83.

Hamill, T.M. and Church, A.T. (2000) Conditional probabilities of significant tornadoes from RUC-2 forecasts. *Weather and Forecasting*, 15, 461–475.

Hopfield, H.S. (1971) Tropospheric effect on electromagnetically measured range prediction from surface weather data. *Radio Science*, 6, 357–367.

Kishore, P., Venkat, R.M., Namboothiric, S.P., Velicognaa, I., Bashab, G., Jiang, J.H., Igarashi, K., Rao, S.V.B. and Sivakumar, V. (2011) Global (50S-50N) distribution of water vapour observed by Cosmic GPS Ro: comparison with GPS radiosonde, NCEP, era-interim, and Jra-25 reanalysis data sets. *Journal of Atmospheric and Solar-Terrestrial Physics*, 73, 1849–1860.

Kouba, J. and Héroux, P. (2001) Precise point positioning using IGS orbit and clock products. *GPS Solutions*, 5, 12–28.

Kuo, Y.H., Schreiner, W.S., Wang, J., Rossister, D.L. and Zhang, Y. (2005) Comparison of GPS radio occultation soundings with radiosondes. *Geophysical Research Letters*, 32, L05817. https://doi.org/10.1029/2004GL021443.

Li, J.G., Mao, J.T. and Li, C.C. (1999) The approach to remote sensing of water vapor based on GPS and linear regression *Tm* in eastern region of China. *Acta Meteorologica Sinica*, 57, 283–292.

Liu, Y.X., Chen, Y.Q. and Liu, J.N. (2000) Determination of weighted mean tropospheric temperature using ground meteorological measurement. *Journal of Wuhan Technical University of Surveying and Mapping*, 25, 400–403.

Lv, Y.P., Yin, H.T. and Huang, D.F. (2008) Modeling of weighted mean atmospheric temperature and application in GPS/PWV of Chengdu region. *Science of Surveying and Mapping*, 33, 103–105.

Ross, R.J. and Rosenfeld, S. (1997) Estimating mean weighted temperature of the atmosphere for Global Positioning System. *Journal of Geophysical Research*, 102, 21719–21730.

Saastamoinen, J. (1972) Atmospheric correction for the Troposphere and stratosphere in radio ranging of satellites in: the use of artificial satellites for geodesy. *Geophysics Monoger*, 15, 247–251.

Schreiner, W., Rochen, C., Sokolovskiy, S., Syndergaard, S. and Hunt, D. (2007) Estimates of the precision of GPS radio occultation from the COSMIC/FORMOSAT-3 mission. *Geophysical Research Letters*, 34, L04808.

University of Wyoming (UWYO). (2018) *45004 Kings Park radiosonde observations*. Available at: http://weather.uwyo.edu/upperair/sounding.html [Accessed 31st November 2018].

Wang, Y., Liu, L.T., Hao, X.G., et al. (2007) The application study of the GPS meteorology network in Wuhan region. Acta Geodaet. Cartogr. *Sinica*, 36, 141–145.

Wang, X., Song, L., Dai, Z. and Cao, Y. (2011) Feature analysis of weighted mean temperature T_m in Hong Kong. *Journal of Nanjing University of Science and Technology*, 3, 47–52.

Yao, Y.B., Zhu, S. and Yue, S.Q. (2012) A globally applicable, season specific model for estimating the weighted mean temperature of the atmosphere. *Journal of Geodesy*, 86, 1125–1135. https://doi.org/10.1007/s00190-012-0568-1.

Yao, Y.B., Zhang, B., Yue, S.Q., Xu, C.Q. and Peng, W.F. (2013) Global empirical model for mapping zenith wet delays onto precipitable water. *Journal of Geodesy*, 87, 439–448. https://doi.org/10.1007/s00190-013-0617-4.

Yao, Y.B., Xu, C.Q., Zhang, B., et al. (2014) GTm_III: a new global empirical model for mapping zenith wet delays onto precipitable water vapour. *Geophysical Journal International*, 197, 202–212.

Zumberge, J.F., Heflin, M.B. and Jefferson, D.C. (1997) Precise point positioning for the efficient and robust analysis of GPS data from large networks. *Journal of Geophysical Research*, 102(B3), 5005–5017.

How to cite this article: Xia P, Ye S, Chen B, Chen D, Xu K. Improving the weighted mean temperature model: A case study using nine year (2007–2015) radiosonde and COSMIC data in Hong Kong. *Meteorol Appl*. 2020;27:e1864. https://doi.org/10.1002/met.1864